Inorg. Chem. **2007**, *46*, 108–116

Insights into the Mechanism of Electrocatalytic Hydrogen Evolution Mediated by $Fe_2(S_2C_3H_6)(CO)_6$: The Simplest Functional Model of the Fe-Hydrogenase Active Site

Claudio Greco,[†] Giuseppe Zampella,[†] Luca Bertini,[†] Maurizio Bruschi,[‡] Piercarlo Fantucci,[†] and Luca De Gioia*,[†]

Department of Biotechnology and Biosciences, University of Milano-Bicocca, Piazza della Scienza 2, 20126 Milan, Italy, and Department of Environmental Science, University of Milano-Bicocca, Piazza della Scienza 1, 20126 Milan, Italy

Received June 27, 2006

The di-iron complex $Fe_2(S_2C_3H_6)(CO)_6$ (**a**), one of the simplest functional models of the Fe-hydrogenases active site, is able to electrocatalyze proton reduction. In the present study, the H_2 evolving path catalyzed by **a** has been characterized using density functional theory. It is showed that, in the early stages of the catalytic cycle, a neutral μ-H adduct is formed; monoelectron reduction and subsequent protonation can give rise to a diprotonated neutral species (**a-μH-SH**), which is characterized by a μ-H group, a protonated sulfur atom, and a CO group bridging the two iron centers, in agreement with experimental IR data indicating the formation of a long-lived μ-CO species. H_2 release from **a-μH-SH**, and its less stable isomer **a-H_2** is kinetically unfavorable, while the corresponding monoanionic compounds (**a-μH-SH$^-$** and **a-H_2^-**) are more reactive in terms of dihydrogen evolution, in agreement with experimental data. The key species involved in electrocatalysis have structural features different from the hypothetical intermediates recently proposed to be involved in the enzymatic process, an observation that is possibly correlated with the reduced catalytic efficiency of the biomimetic di-iron assembly.

Introduction

The perspective of using molecular hydrogen as a clean energy carrier in the future is stimulating scientists toward the development of novel, cheap, and ecocompatible processes for H_2 production and oxidation.[1] In particular, the design of inexpensive electrocatalytic materials could take advantage from the study of hydrogenases, a class of metalloenzymes that play a fundamental role in microbial hydrogen metabolism.[2] Hydrogenases can be subdivided into three different families: Ni−Fe hydrogenases, whose active site contains a nickel and an iron atom; Fe-hydrogenases, that include only iron ions as cofactors; and another family of iron-containing hydrogenases for which, however, few structural data are presently available.[3]

The Fe-hydrogenases active site contains a peculiar {2Fe2S} iron−sulfur cluster linked to a classical Fe_4S_4 cubane via a cysteinyl sulfur ligand (Scheme 1). The resulting {6Fe6S} complex is usually referred to as the H-cluster. The coordination environment of the two iron atoms in the {2Fe2S} subcluster includes carbonyl and cyanide ligands, and also a bidentate $S-X_3-S$ ligand, where X_3 is composed of covalently linked light atoms.[4] The nature of the X atoms is still an object of debate, and both propane-1,3-dithiolate (PDT) and di(thiomethyl)amine (DTMA) have been proposed

* Corresponding author. E-mail: luca.degioia@unimib.it. Fax. +39. 02.64483478.
[†] Department of Biotechnology and Biosciences.
[‡] Department of Environmental Science.

(1) Darensboug, M. Y. *Nature* **2005**, *433*, 589.
(2) Albracht, S. P. *Biochim. Biophys. Acta* **1994**, *167*, 1188. Graf, E. G.; Thauer, R. K. *FEBS Lett.* **1981**, *136*, 165. Adams, M. W. W. *Biochim. Biophys. Acta* **1990**, *115*, 1020. Cammack, R. *Nature* **1999**, *397*, 214. Nicolet, Y.; Lemon, B. J.; Fontecilla-Camps, J. C.; Peters, J. W. *Trends Biochem. Sci.* **2000**, *25*, 138. Peters, J. W. *Curr. Opin. Struct. Biol.* **1999**, *9*, 670. Horner, D. S.; Heil, B.; Happe, T.; Embley, T. M. *Trends Biochem. Sci* **2002**, *27*, 148. Nicolet, Y.; Cavazza, C.; Fontecilla-Camps, J. C. *J. Inorg. Biochem.* **2002**, *91*, 1. *Hydrogen as Fuel*—Learning from Nature; Cammack, R., Frey, M., Robson, R., Eds.; Taylor and Francis: London, 2001. Armstrong, F. A. *Curr. Opin. Chem. Biol.* **2004**, *8*, 133.
(3) Lyon, E. J.; Shima, S.; Buurman, G.; Chowdhuri, S.; Batschauer, A.; Steinbach, K.; Thauer, R. K. *Eur. J. Biochem.* **2004**, *271*, 195. Pilak, O.; Mamat, B.; Vogt, S.; Hagemeier, C. H.; Thauer, R. K.; Shima, S.; Vonrhein, C.; Warkentin, E.; Ermler, U. *J. Mol. Biol.* **2006**, *358*, 798.
(4) Nicolet, Y.; Piras, C.; Legrand, P.; Hatchikian, E. C.; Fontecilla-Camps, J. C. *Structure* **1999**, *7*, 13. Peters, J. W.; Lanzilotta, W. N.; Lemon, B. J.; Seefeldt, L. C. *Science* **1998**, *282*, 1853. Nicolet, Y.; de Lacey, A. L.; Vernede, X.; Fernandez, V. M.; Hatchikian, E. C.; Fontecilla-Camps, J. C. *J. Am. Chem. Soc.* **2001**, *123*, 1596.

10.1021/ic061168+ CCC: $37.00
Published on Web 12/10/2006

Scheme 1. Structure of the H-cluster Found in Fe-Hydrogenases

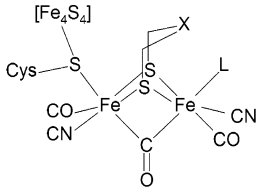

as plausible bidentate ligands for the enzymatic cofactor. The iron ion distal to the Fe_4S_4 moiety has a labile coordination site (L), which is thought to be occupied by either H_2 or H^- during catalysis. Moreover, experimental[5] and theoretical[6] investigations indicate that the binuclear cluster changes redox state during the catalytic cycle.

Insight into electronic and structural features of the Fe-hydrogenases active site has stimulated experimental chemists toward the synthesis of biomimetic iron−sulfur complexes that can maintain the catalytic properties of Fe-hydrogenases.[7] Among the synthetic assemblies obtained so far, the species $Fe_2(S_2C_3H_6)(CO)_6$ can be considered as one of the simplest functional models of the {2Fe2S} binuclear subsite. Further efforts led to the synthesis of model complexes with different ligands around the metal centers: in particular, PDT-containing di-iron complexes that include cyanide and/or phosphine ligands have been obtained,[8,9] while recently the synthesis of a N-heterocyclic carbene substituted model compound was described.[10] Pickett and collaborators have recently reported the synthesis of a hexacarbonyl Fe_6S_6 complex that reproduces the main features of the entire H-cluster.[11] Remarkably, all the above-mentioned model compounds, together with other related complexes including DTMA derivatives, proved to be able to catalyze the electrochemical reduction of protons, leading to H_2 production.[11−14] In particular, cyclic voltammetry

Scheme 2. Reaction Scheme[a] for the Dihydrogen-Evolving Processes As Experimentally Characterized by Pickett et al.[12,13]

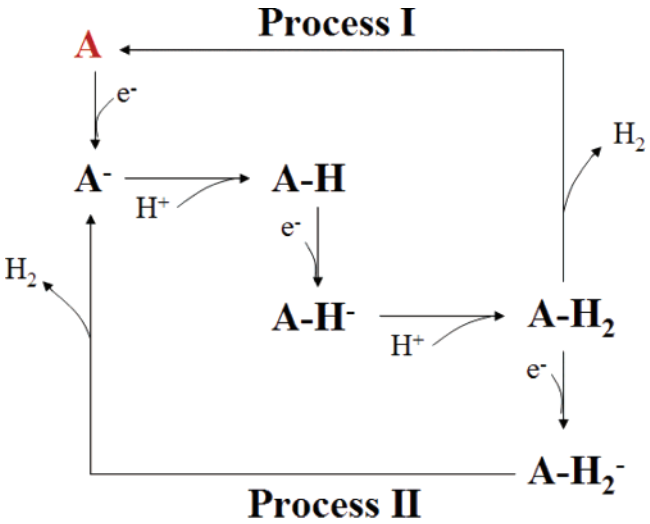

[a] Species experimentally characterized by X-ray diffraction are shown in red.

experiments have shown that acetonitrile solutions of $Fe_2(S_2C_3H_6)(CO)_6$ can catalyze dihydrogen evolution.[8,12,13] The results of combined spectroscopic/electrochemical investigations for the reduction of $Fe_2(S_2C_3H_6)(CO)_6$ in the presence of *p*-toluene-sulfonic acid (HOTs) led to the formulation of the following reaction scheme (Scheme 2):[12,13] the $Fe_2(S_2C_3H_6)(CO)_6$ complex (**A**, a Fe(I)Fe(I) neutral species) undergoes monoelectronic reduction leading to $\mathbf{A}^-$. Addition of HOTs to the reaction environment results in protonation of $\mathbf{A}^-$; the protonated complex (**A-H**) can undergo a second monoelectronic reduction, giving rise to the adduct $\mathbf{A\text{-}H}^-$. Finally, protonation of $\mathbf{A\text{-}H}^-$ leads to the transient species $\mathbf{A\text{-}H_2}$, preceding molecular hydrogen evolution and closure of the catalytic cycle (process I). The diprotonated adduct ($\mathbf{A\text{-}H_2}$) can also be further reduced, a reaction step which is again followed by H_2 production (process II).

It was possible to distinguish between the two hydrogen evolving processes because process I takes place at less negative potentials relative to those of process II ($E_I = -1.12$V versus $E_{II} = -1.34$V). Notably, H_2 production is much faster in the latter case: in fact, the estimated values of the forward kinetic constants for the final reaction in processes I and II (i.e., reactions $\mathbf{A\text{-}H_2} \rightarrow H_2 + \mathbf{A}$ and $\mathbf{A\text{-}H_2}^- \rightarrow H_2 + \mathbf{A}^-$) are 4 and 10^4, respectively.[12,13] Moreover, IR spectroscopic data are consistent with the formation of a structurally uncharacterized mono- or diprotonated μ-CO intermediate species, which might be catalytically relevant.[12,13] However, among all the intermediates formed in the catalytic cycle, it was possible to characterize thoroughly only the structural features of the parent complex **A**, while the short lifetime of mono- and diprotonated species did not allow us to fully unravel their properties.

Prompted by these observations, we have carried out a density functional theory (DFT) study of the H_2 evolving process, in order to dissect the mechanism leading to

(5) Pierik, A. J.; Hagen, W. R.; Redeker, J. S.; Wolbert, R. B. G.; Boersma, M.; Verhagen, M.; Grande, H. J.; Veeger, C.; Mutsaers, P. H. A.; Sands, R. H.; Dunham, W. R. *Eur. J. Biochem.* **1992**, *209*, 63. Zambrano, I. C.; Kowal, A. T.; Mortenson, L. E.; Adams, M. W. W.; Johnson, M. K. *J. Biol. Chem.* **1989**, *264*, 20974. Adams, M. W. W. *J. Biol. Chem.* **1987**, *262*, 15054. Adams, M. W. W.; Mortenson, L. E. *J. Biol. Chem.* **1984**, *259*, 7045. Bennett, B.; Lemon, B. J.; Peters, J. W. *Biochemistry* **2000**, *39*, 7455. Lemon, B. J.; Peters, J. W. *J. Am. Chem. Soc.* **2000**, *122*, 3793−3794. Kowal, A. T.; Adams, M. W. W.; Johnson, M. K. *J. Biol. Chem.* **1989**, *264*, 4342. Rusnak, F. M.; Adams, M. W. W.; Mortenson, L. E.; Munck, E. *J. Biol. Chem.* **1987**, *262*, 38.

(6) Cao, Z.; Hall, M. B. *J. Am. Chem. Soc.* **2001**, *123*, 3734. Fan, H.-J.; Hall, M. B. *J. Am. Chem. Soc.* **2001**, *123*, 3828. Liu, Z.-P.; Hu, P. *J. Am. Chem. Soc.* **2002**, *124*, 5175. Bruschi, M.; Fantucci, P.; De Gioia, L. *Inorg. Chem.* **2003**, *42*, 4773.

(7) Capon, J.-F.; Gloaguen, F.; Schollhammer, P.; Talarmin, J. *Coord. Chem. Rev.* **2005**, *249*, 1664.

(8) Chong, D.; Georgakaki, I. P.; Mejia-Rodriguez, R.; Sanabria-Chinchilla, J.; Soriaga, M. P.; Darensbourg, M. Y. *Dalton Trans.* **2003**, 4158.

(9) Gloaguen, F.; Lawrence, J. D.; Rauchfuss, T. B. *J. Am. Chem. Soc.* **2001**, *123*, 9476. Gloaguen, F.; Lawrence, J. D.; Rauchfuss, T. B.; Benard, M.; Rohmer, M. *Inorg. Chem.* **2002**, *41*, 6573.

(10) Tye, J. W.; Lee, J.; Wang, H.; Mejia-Rodriguez, R.; Reibenspies, J. H.; Hall, M. B.; Darensbourg, M. Y. *Inorg. Chem.* **2005**, *44*, 5550.

(11) Tard, C; Liu, X; Ibrahim, S. K.; Bruschi, M.; De Gioia, L; Davies, S. C.; Yang, X.; Wang, L. S.; Sawers, G.; Pickett, C. J. *Nature* **2005**, *433*, 610.

(12) Borg, S. J.; Behrsing, T.; Best, S. P.; Razavet, M.; Liu, X.; Pickett, C. J. *J. Am. Chem. Soc.* **2004**, *126*, 16988.

(13) Borg, S. J.; Bondin, M. I.; Best, S. P.; Razavet, M.; Liu, X.; Pickett, C. J. *Biochem. Soc. Trans.* **2005**, *33*, 3.

(14) Gao, W.; Liu, J.; Ma, C.; Weng, L.; Jin, K.; Chen, C.; Åkermark, B.; Sun, L. *Inorg. Chim. Acta* **2006**, *359*, 1071.

dihydrogen production and disclose the structural and electronic properties of key intermediate species formed in the catalytic cycle.

As a first step, we validated the computational approach by comparing DFT structures and UV−vis and IR spectra with the corresponding experimental data currently available.[15] Then, we studied the structural properties of complex $\mathbf{A}^-$, and the path leading to the monoprotonated complexes **A-H** and $\mathbf{A\text{-}H}^-$, showing that the formation of μ-H adducts is favored in the first part of process I. Subsequently, we investigated the diprotonated neutral species $\mathbf{A\text{-}H_2}$, showing that this species corresponds to a μ-H adduct protonated on one of the PDT sulfur atoms and featuring also a μ-CO group. These results have also allowed us to rationalize the IR experimental data indicating the formation of a long-lived μ-CO species during the catalytic cycle. Finally, the structure and reactivity of $\mathbf{A\text{-}H_2}^-$, which is formed in process II, have been investigated.

Methods

DFT calculations have been carried out using the pure functional BP86[16] and a valence triple-ζ basis set with polarization on all atoms (TZVP).[17] Calculations have been carried out with the TURBOMOLE 5.7 suite[18] applying the resolution-of-the-identity technique.[19]

Stationary points of the energy hypersurface have been located by means of energy gradient techniques, and full vibrational analysis has been carried out to further characterize each stationary point.

The optimization of transition state structures has been carried out according to a procedure based on a pseudo-Newton−Raphson method. Initially, geometry optimization of a guessed transition state structure is carried out constraining the distance corresponding to the reaction coordinate. Vibrational analysis, at the BP86/TZVP level, of the constrained minimum energy structures is then carried out, and if one negative eigenmode corresponding to the reaction coordinate is found, the curvature determined at such a point is used as a starting point in the transition state search. The search of the transition state structure is carried out using an eigenvector-following algorithm: the eigenvectors in the Hessian are sorted in ascending order, the first one being that associated with the negative eigenvalue. After the first step, the search is performed by choosing the critical eigenvector with a maximum overlap criterion, which is based on the dot product with the eigenvector followed at the previous step. Finally, the analytical Hessian matrix is calculated to carry out the vibrational analysis of the stationary point.

Free energy (G) values have been obtained from the electronic SCF energy considering three contributions to the total partition function (Q), namely $q_{\text{translational}}$, $q_{\text{rotational}}$, and $q_{\text{vibrational}}$, under the assumption that Q may be written as the product of such terms.[20] In order to evaluate enthalpy and entropy contributions, the values of temperature, pressure, and scaling factor for the SCF wavenumbers have been set to 298.15 K, 1 bar, and 0.9914, respectively.

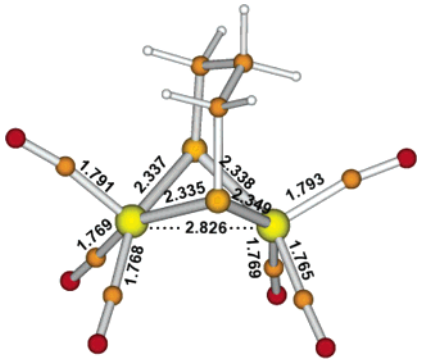

Figure 1. Optimized structures of $\mathbf{a}^-$. Selected distances are given in ångstroms.

Scheme 3. Schematic Structure of the Formyl $\mathbf{A1\text{-}H}^-$ Species

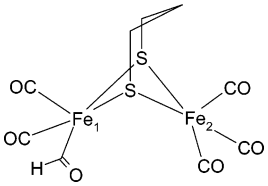

Rotations have been treated classically, and vibrational modes have been described according to the harmonic approximation.

The effect of the solvent (acetonitrile, $\epsilon = 36.64$) has been evaluated according to the COSMO approach.[21]

Calculations of reduction potentials have been carried out using the Nernst equation, $\Delta G = -nFE$, where n is the number of electrons transferred and F is the Faraday constant. The resulting E value is an absolute reduction potential (E^{abs}); i.e., it is not referenced to any standard electrode. Therefore, in order to obtain the calculated reduction potentials (E^{calc}'s), the absolute reduction potential for the SCE (4.671 V)[22] has been systematically subtracted from E^{abs} values. Both proton binding energies and E^{calc} values have been computed taking into account solvation contributions.

Excitation energies have been computed within the time-dependent DFT (TDDFT) formalism, as implemented in TURBOMOLE 5.7.[23] In each case, at least 40 equal spin multiplicity excited states have been calculated. Computed UV spectra have been obtained centering Gaussian curves with amplitude = 18 nm on the transition frequencies.

Results and Discussion

Validation of the Computational Method. Initially, with the aim of validating the DFT approach (BP86/TZVP, see Methods section), we have investigated relevant species that have been thoroughly characterized experimentally. Indeed, DFT methods are known to generally give a good account of the structures of models of the Fe-hydrogenase active site. However, computed relative energies and spectroscopic properties have to be taken with more caution. As a consequence, whenever possible we have compared our theoretical results with the corresponding experimental data.

(15) Fiedler, A. T.; Brunold, T. C. *Inorg. Chem.* **2005**, *44*, 1794.
(16) Becke, A. D. *Phys. Rev. A* **1988**, *38*, 3098. Perdew, J. P. *Phys. Rev. B* **1986**, *33*, 8822.
(17) Schafer, A.; Huber, C.; Ahlrichs, R. *J. Chem. Phys.* **1994**, *100*, 5829.
(18) Ahlrichs, R.; Bar, M.; Haser, M.; Horn, H.; Kolmel, C. *Chem. Phys. Lett.* **1989**, *162*, 165.
(19) Eichkorn, K.; Weigend, F.; Treutler, O.; Ahlrichs, R. *Theor. Chem. Acc.* **1997**, *97*, 119.
(20) Jensen, F. *Introduction to Computational Chemistry*; John Wiley & Sons Ltd: Chichester, U.K.
(21) Klamt, A. *J. Phys. Chem.* **1995**, *99*, 2224. Klamt, A. *J. Phys. Chem.* **1996**, *100*, 3349.
(22) Reiss, H.; Heller, A. *J. Phys. Chem.* **1985**, *89*, 4207. Harris D. C.; *Quantitative Chemical Analysis*; W. H. Freeman & Company: New York, 1987.
(23) Furche, F.; Ahlrichs, R. *J. Chem. Phys.* **2002**, *117*, 7433. Grimme, S.; Furche, F.; Ahlrichs, R. *Chem. Phys. Lett.* **2002**, *361*, 321. Weiss, H.; Ahlrichs, R.; Haser, M. J. *Chem. Phys.* **1993**, *99*, 1262. Bauernschmitt, R.; Ahlrichs, R. *J. Chem. Phys.* **1996**, *104*, 9047.

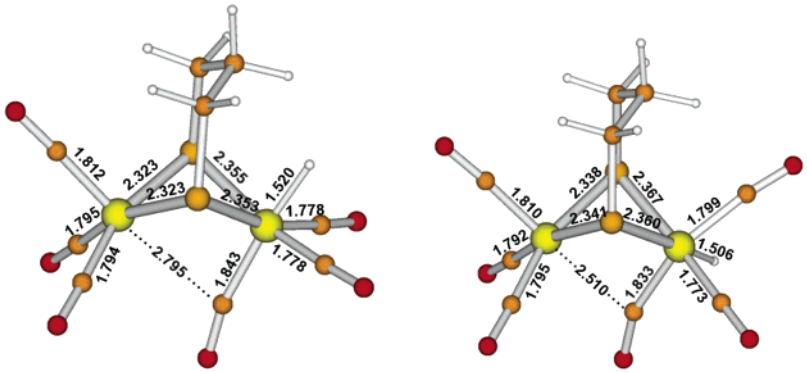

a2-H **a3-H**

Figure 2. Optimized structures of **a2-H** and **a3-H**. Selected distances are given in ångstroms.

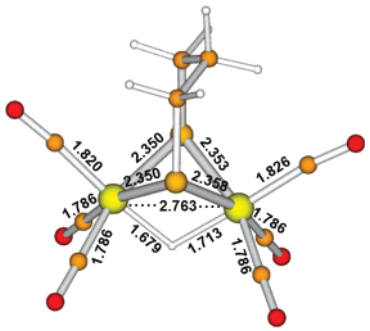

a-μH

Figure 3. Optimized structures of **a-μH**. Selected distances are given in ångstroms.

Table 1. Computed Relative Stabilities of Isomers Obtained upon $\mathbf{a}^-$ Protonation[a]

a-μH	**a1-H**	**a2-H**	**a3-H**	**a-SH**
0.0	16.0	8.3	11.4	8.1

[a] Energy values in kcal mol^{-1}. The DFT structures of **a1-H** and **a-SH** are available as Supporting Information.

The structures of **A** and $[Fe_2(S_2C_3H_6)(CO)_5(HCO)]^-$, a formyl adduct obtained from the reaction between **A** and hydrides ($\mathbf{A1\text{-}H}^-$; Scheme 3), were experimentally characterized by EXAFS, IR, and UV−vis spectroscopy.[12−15] Moreover, the geometry of **A** was determined by X-ray diffraction.[24] In addition, both infrared and UV−vis spectroscopy data are available for **A** and $\mathbf{A1\text{-}H}^-$.[12−15]

Hereafter, for the sake of clarity, we will designate the calculated and experimental complexes by lower- and uppercase bold letters, respectively. We will also distinctly refer to the two iron ions of the investigated complexes: "Fe1" will refer to the iron atom distal to the β carbon atom of the PDT ligand, while "Fe2" indicates the proximal metal center (see Scheme 3).

The comparison between the optimized geometry of **a** (see Supporting Information; Figure 1S) and X-ray data shows that computed bond lengths are all within ±0.035 Å of those determined by crystallography, except for Fe−S distances, which differ from experimental values by 0.04 Å (see Supporting Information, Table 1S). A similarly good match was found when bond lengths in **a** and $\mathbf{a1\text{-}H}^-$ were compared to the corresponding EXAFS values for **A** and $\mathbf{A1\text{-}H}^-$: in this case, the largest difference is observed for Fe−Fe distances, for which the computed values are overestimated by about 0.08 Å.

As a second step of the validation procedure, we have compared experimental and computed vibrational frequencies of CO groups in **A** and $\mathbf{A1\text{-}H}^-$, as well as UV−vis spectra (see Supporting Information, Table 1S and Figure 1S). The good agreement between computational and experimental spectroscopic data gives further support to the quality of the adopted level of theory.

Process I: Monoelectron Reduction of A. As outlined in the Introduction, the catalytic cycle for hydrogen evolution, proposed on the ground of experimental data,[12,13] starts with the monoelectronic reduction of **A**, leading to $\mathbf{A}^-$. The latter compound has been experimentally characterized by UV−vis and IR spectroscopy, but no X-ray or EXAFS data are available for this species.

Similar to **a**, the coordination geometry of the iron ions in the DFT optimized species $\mathbf{a}^-$ is square pyramidal (Figure 1). However, the $\mathbf{a} + e^- \rightarrow \mathbf{a}^-$ reduction reaction is accompanied by a 0.28 Å lengthening of the Fe−Fe distance, an observation which suggests cleavage of the Fe−Fe bond in the anionic complex.

A comparison between experimental and computed CO stretching frequencies for $\mathbf{A}^-$ and $\mathbf{a}^-$ highlights a very high correlation ($R^2 = 0.982$, see also Supporting Information), and a similarly good match was found when electronic excitation data were taken into account (see Supporting Information, Figure 2S). Such results allow us to conclude that $\mathbf{a}^-$ corresponds to the experimentally characterized intermediate species $\mathbf{A}^-$.

Process I: Proton Binding to $\mathbf{A}^-$. Complex $\mathbf{A}^-$ is the first proton acceptor species in the course of catalysis, leading to the structurally uncharacterized species **A-H** (Scheme 2). Notably, FT-IR data collected during the reduction reaction of **A** in a protic environment evidenced the formation of a μ-CO species, an observation that might imply the presence of a terminal hydride in **A-H**. The thorough evaluation of this possibility is very relevant for the design of novel

(24) Lyon, E. J.; Georgakaki, I. P.; Reibenspies, J. H.; Darensbourg, M. Y. *Angew. Chem., Int. Ed.* **1999**, *38*, 3178.

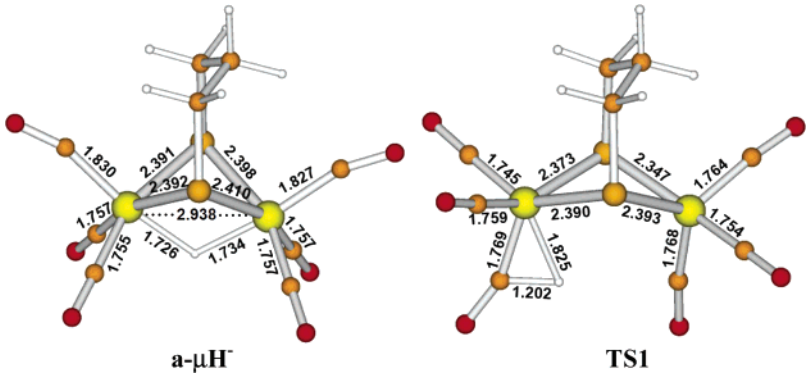

Figure 4. Optimized structures of **a**-μ**H**$^-$ and of the transition state for the reaction **a**-μ**H**$^-$ → **a1-H**$^-$. Selected distances are given in ångstroms.

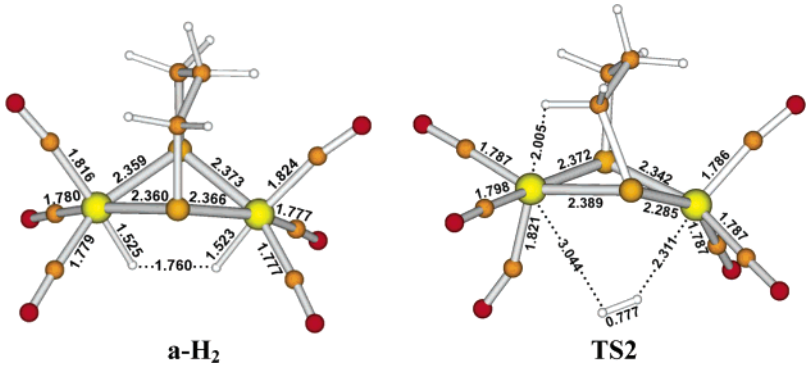

Figure 5. Optimized structures of **a-H$_2$** and of the corresponding transition state leading to H_2 evolution. Selected distances are in given in ångstroms.

Scheme 4. Starting Structure Used for Geometry Optimization of the **a-H$_2$** Model Complex

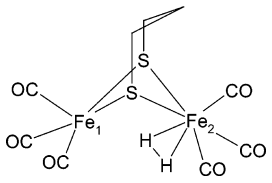

catalysts because a terminal hydride is expected to be more reactive toward H^+ than a μ-H ligand.[25] Formation of a terminal hydride species has been proposed to be relevant also in the Fe-hydrogenases catalytic cycle.[26] Prompted by these observations, we have optimized the structures of several plausible **A-H** isomers. Initially, structures featuring a bridging CO group and a terminal hydride bound to Fe2 were taken into account (**a2-H** and **a3-H**, Figure 2). The difference between **a2-H** and **a3-H** stands in the position of the hydride ligand, which is *trans* to the μ-CO group in the former compound, while in the latter it is *trans* to one of the sulfur atoms of PDT.

In **a2-H** and **a3-H** the carbonyl ligand that bridges the two metal centers can be best described as "semibridging" (C−Fe2 = 1.843 Å in **a2-H** and 1.833 Å in **a3-H**; C−Fe1 = 2.795 Å and 2.510 Å in **a2-H** and **a3-H**, respectively). In fact, the computed vibrational frequencies for **a2-H** and **a3-H** corresponding to the stretching of the bridging CO group (1915 and 1944 cm^{-1} in **a2-H** and **a3-H**, respectively) are very different from that expected for a "canonical" μ-CO species. Similar results were obtained at the B3LYP/TZVP level of theory (data not shown). Therefore, it can be concluded that the μ-CO species detected during catalysis cannot correspond to monoprotonated neutral complexes featuring a terminal hydride ligand.

Protonation of **a**$^-$ might give rise to an adduct featuring a hydride bridging the metal centers. Indeed, biomimetic μ-H di-iron complexes have been experimentally characterized,[27] and previous theoretical studies on complexes structurally related to $Fe_2(S_2C_3H_6)(CO)_6$ have shown that the formation of μ-H adducts is thermodynamically favorable.[28] Therefore, another plausible candidate for the **A-H** intermediate is **a**-μ**H** (Figure 3), which includes a μ-hydride and six terminal carbonyl ligands. As a matter of fact, it turned out that **a**-μ**H** is the best candidate for the product of **A**$^-$ protonation (**A-H**, Scheme 2): this assignment is supported by the stability of **a**-μ**H** relative to **a2-H** and **a3-H** ($\Delta G_{(\mathbf{a}-\mu\mathbf{H})-(\mathbf{a2}-\mathbf{H})} = -8.3$ kcal mol^{-1}; $\Delta G_{(\mathbf{a}-\mu\mathbf{H})-(\mathbf{a3}-\mathbf{H})} = -11.4$ kcal mol^{-1}). Moreover, **a**-μ**H** is also significantly more stable than other protonation products derived from **a**$^-$ (Table 1 and Supporting Information).

Process I: Monoelectron Reduction of A-H. The next step in the catalytic cycle is the monoelectronic reduction

(25) Justice, A. K.; Linck, R. C.; Rauchfuss, T. B.; Wilson, S. R. *J. Am. Chem. Soc.* **2004**, *126*, 13214.
(26) Bruschi, M.; Zampella, G.; Fantucci, P.; De Gioia, L. *Coord. Chem. Rev.* **2005**, *249*, 1664.
(27) Le Borgne, G.; Grandjean, D.; Mathieu, R.; Poilblanc, R. *J. Organomet. Chem.* **1977**, *131*, 429. Zhao, X.; Georgakaki, I. P.; Miller, M. L.; Yarbrough, J. C.; Darensbourg, M. Y. *J. Am. Chem. Soc.* **2001**, *123*, 9710.
(28) Bruschi, M.; Fantucci, P.; De Gioia, L. *Inorg. Chem.* **2002**, *41*, 1421.

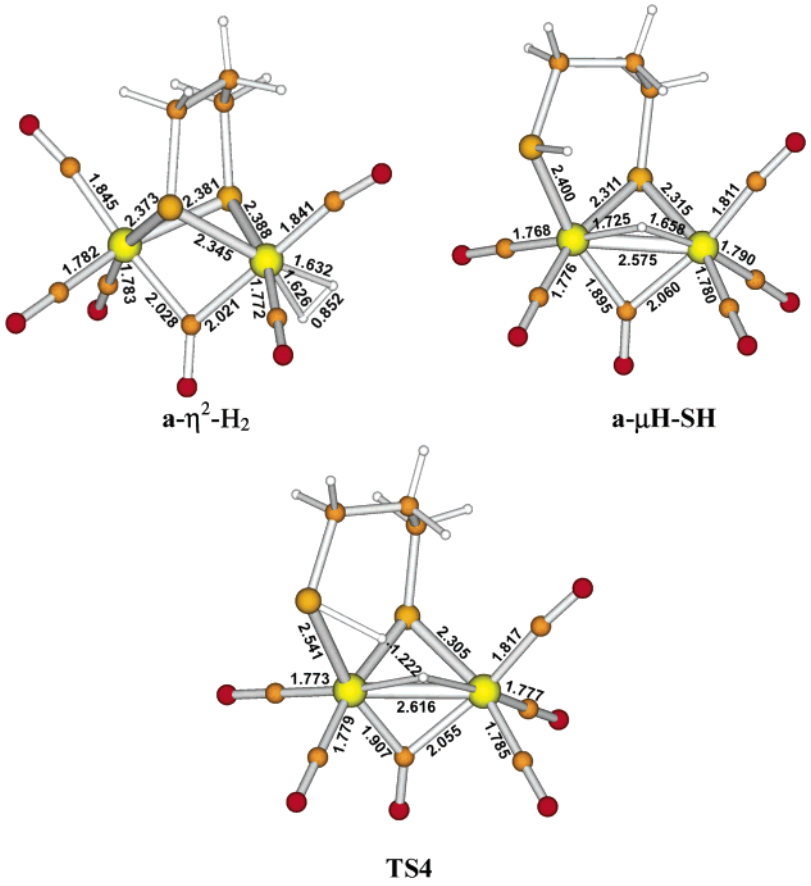

Figure 6. Optimized structures of **a-η^2-H$_2$** and **a-μH−SH**, as well as the transition state for H_2 evolution from **a-μH-SH** (**TS4**). Selected distances are given in ångstroms.

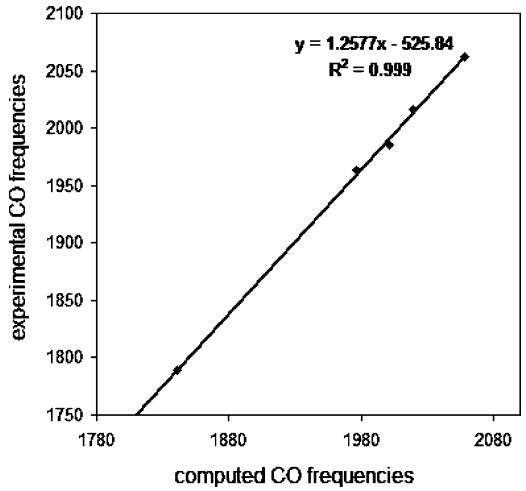

Figure 7. Linear fitting of the calculated and experimental CO frequencies for the CO-bridged adduct **a-μH-SH**.

of **A-H**, leading to the formally Fe(I)Fe(I) species **A-H**$^-$ (Scheme 2), for which different isomers are conceivable. Addition of one electron to **a-μH** results in a structure which is still characterized by the presence of a bridging hydride (complex **a-μH**$^-$, Figure 4), even though Fe−Fe and Fe−H distances become longer than those observed in **a-μH**.

Among the other isomers, it turned out that only the formyl species **a1-H**$^-$ (see Supporting Information) is more stable than **a-μH**$^-$ ($\Delta G_{(\mathbf{a}-\mu\mathbf{H}^-)-(\mathbf{a1}-\mathbf{H}^-)} = 9.6$ kcal mol^{-1}; $\Delta G_{(\mathbf{a}-\mu\mathbf{H}^-)-(\mathbf{a2}-\mathbf{H}^-)} = -3.0$ kcal mol^{-1}; $\Delta G_{(\mathbf{a}-\mu\mathbf{H}^-)-(\mathbf{a3}-\mathbf{H}^-)} = -2.5$ kcal mol^{-1}; see also Supporting Information). This observation may suggest that **a-μH**$^-$ can spontaneously rearrange to **a1-H**$^-$. However, it should be noted that **A1-H**$^-$ can be obtained only as a product of the reaction between **A** and hydrides,[12] and there is no experimental evidence for the formation of formyl-containing complexes during the electrocatalytic processes. Therefore, the comparison between experimental and computational results suggests that the free energy barrier between **a-μH**$^-$ and **a1-H**$^-$ can be sufficiently high to hinder the interconversion. To probe this hypothesis, we have optimized the transition state structure for the reaction **a-μH**$^-$ → **a1-H**$^-$; the resulting structure (**TS1**, see Figure 4) is characterized by a 60° rotation of the ligands around Fe1, relative to the geometry observed in **a-μH**$^-$. The conversion from **a-μH**$^-$ to **a1-H**$^-$ is characterized by a free energy barrier ($\Delta G^{\ddagger} = 11.4$ kcal mol^{-1}) that is not sufficiently low to allow this process: in fact, in a protic environment the rearrangement **a-μH**$^-$ → **a1-H**$^-$ is in competition with the protonation of the monoanionic complex (**A-H**$^-$ + H$^+$ → **A-H$_2$**), which takes place very rapidly.[12,13] As a consequence, the reduction step leading to **a-μH**$^-$ is expected to be immediately followed by the protonation of this anionic species, thus removing **a-μH**$^-$ from the equilibrium **a-μH**$^-$ → **a1-H**$^-$.

Process I: Proton Binding to A-H$^-$**.** On the basis of the results discussed above, complex **a-μH**$^-$ is the species that undergoes the second protonation step during the catalytic cycle, leading to a compound that corresponds to the

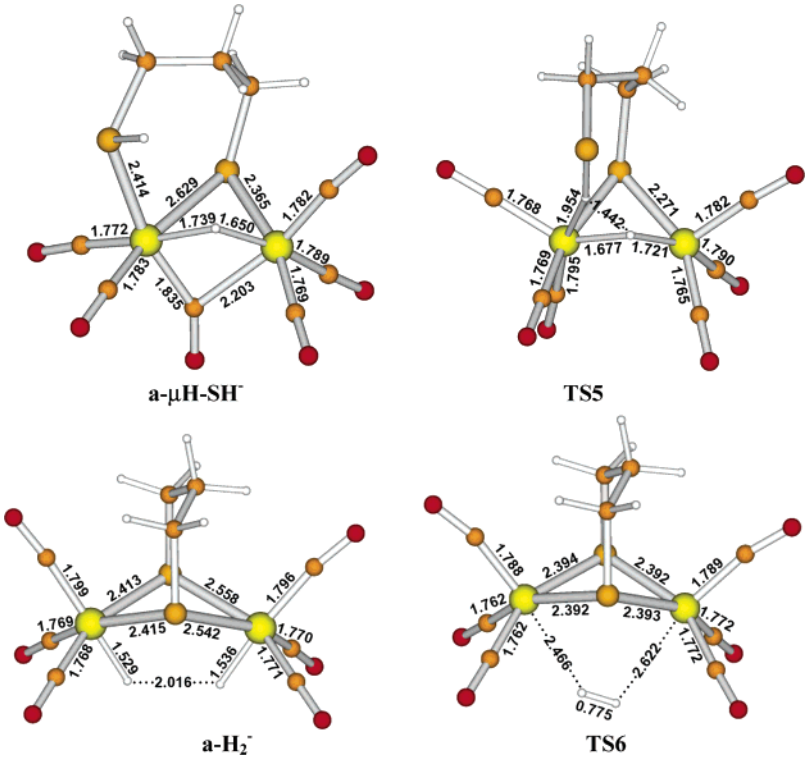

Figure 8. Optimized structures of **a**-μ**H-SH**$^-$, the transition state for H_2 evolution from **a**-μ**H-SH**$^-$ (**TS5**), **a-H**$_2^-$, and the transition state for H_2 evolution from **a-H**$_2^-$ (**TS6**). Selected distances are given in ångstroms.

Table 2. Experimental and Computed Redox Potentials (V) for Relevant Monoelectron Reduction Reactions

	redox potential (exptl)[12,13]	redox potential (computed)
a → **a**$^-$	−1.2	−1.26
a-μ**H** → **a**-μ**H**$^-$	−1.1	−1.16
a-μ**H-SH** → **a**-μ**H-SH**$^-$	−1.45	−1.50

experimentally characterized species **A-H$_2$** (Scheme 2). The addition of a proton to **a**-μ**H**$^-$ could, at least in principle, lead again to different isomers. An adduct featuring a dihydrogen molecule coordinated to one of the iron ions (see Scheme 4) does not correspond to an energy minimum and during optimization evolved to a species featuring two separate hydrogen atoms terminally bound to each metal center (complex **a-H$_2$**, Figure 5). In **a-H$_2$**, the coordination sphere of both iron centers is octahedral, and the H−H and Fe−Fe distances are very large (1.760 and 3.397 Å, respectively). **a-H$_2$** is by far less stable than the van der Waals adduct between **a** and H_2 (ΔG = 35.3 kcal mol^{-1}), indicating that molecular hydrogen release from **a-H$_2$** is a thermodynamically favorable process.

In order to gain insights into the reactivity of **a-H$_2$**, we have characterized the transition state for the reaction leading to H_2 production (**TS2**, Figure 5). In **TS2** the approach of hydrogen atoms toward each other is allowed by the lengthening of Fe−H bonds. The formation of the H−H bond is also accompanied by a conformational rearrangement of the alkyl chain of PDT, bringing one of the hydrogen atoms of the bidentate ligand closer to Fe1. The computed free energy barrier for H_2 formation is quite large (23.0 kcal mol^{-1}), even though it should be noted that the computed value is expected to be overestimated (see Supporting Information).

Another plausible candidate for **A-H$_2$** is [Fe$_2$(S$_2$C$_3$H$_6$)(CO)$_6$H$_2$], which features a μ-CO group and a dihydrogen molecule *trans* to a sulfur atom of PDT (**a**-η^2-H$_2$, Figure 6). Notably, the CO vibrational frequencies computed for **a**-η^2-**H$_2$** are very similar to those reported for the experimentally detected μ-CO species (R^2 = 0.990, see Supporting Information). However, it should be noted that the μ-CO intermediate characterized experimentally is a long-lived species in the absence of reducing potential ($t_{1/2} \geq$ 5s).[13] In fact, **a**-η^2-**H$_2$** is less stable than **a-H$_2$** by 5.6 kcal mol^{-1}, and therefore, it should be present in a very small amount in solution. Moreover, the transition state corresponding to dihydrogen evolution from **a**-η^2-**H$_2$** (**TS3**, see Supporting Information) is associated with a free energy barrier of 11.8 kcal mol^{-1}, leading to the conclusion that **a**-η^2-**H$_2$** cannot be a long-lived species at room temperature.

The DFT optimization of other plausible diprotonated neutral species led to the characterization of **a**-μ**H-SH** (Figure 6), which features a protonated sulfur atom coordinated only to one Fe center and both a hydride and a carbonyl ligand bridging the two iron atoms. In this context, it is important to note that protonation of a sulfur atom in the bidentate ligand was already proposed to be relevant in the mechanism leading to H_2 evolution,[6,28] and it has been recently observed experimentally in a model complex structurally related to Fe$_2$(S$_2$C$_3$H$_6$)(CO)$_6$.[29] Most importantly, **a**-μ**H-SH** is significantly more stable than **a-H$_2$** (ΔG =

(29) Dong, W.; Wang, M.; Liu, X.; Jin, K.; Li, G.; Wang, F.; Sun, L. *Chem. Commun.* **2006**, 305.

Scheme 5. Refined Reaction Scheme for the Dihydrogen-Evolving Processes

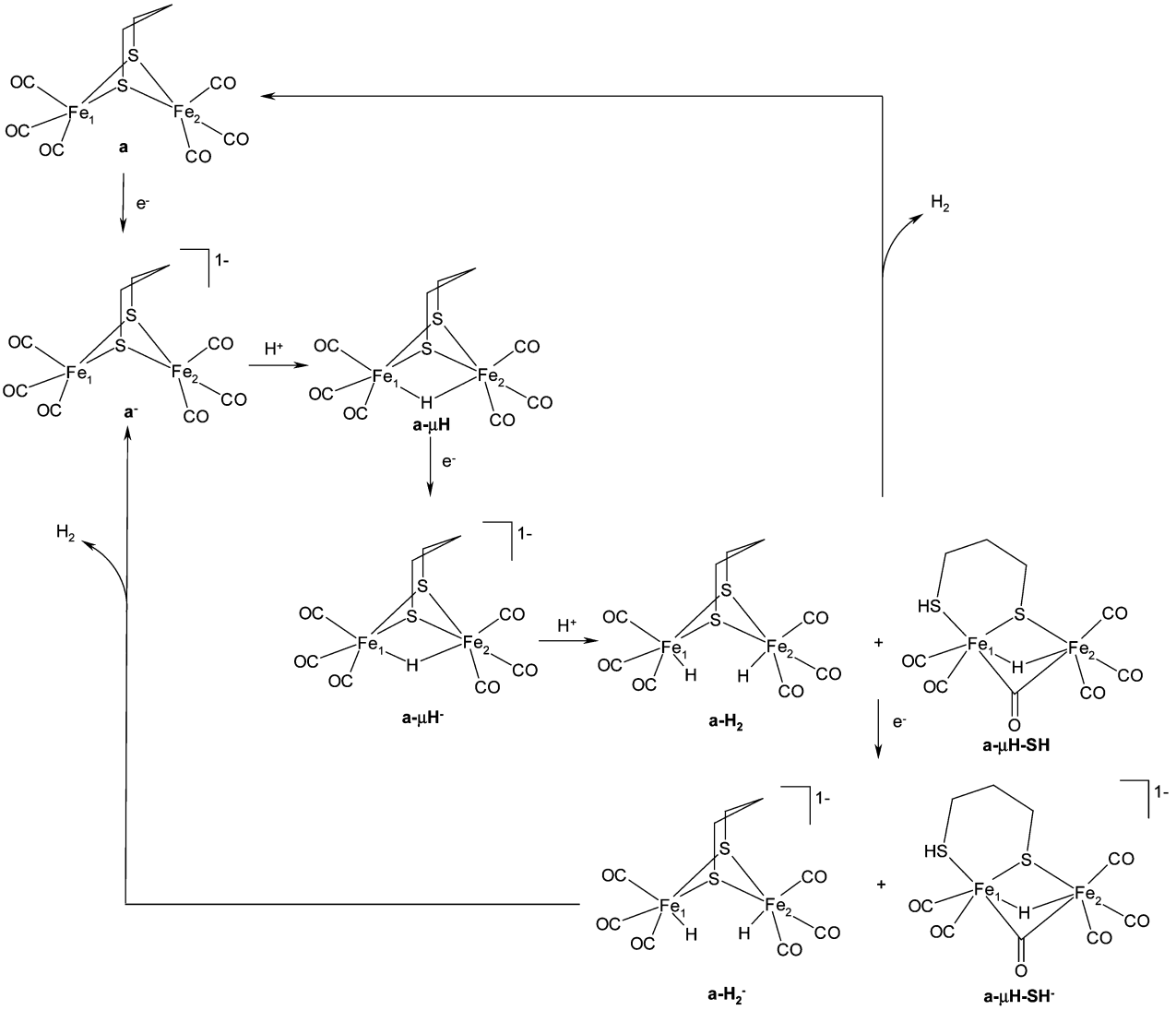

-14.6 kcal mol^{-1}) and **a-η^2-H$_2$** ($\Delta G = -20.2$ kcal mol^{-1}). Moreover, **a-μH-SH** features computed vibrational frequencies that are in very close agreement with the experimental data collected for the unidentified μ-CO adduct (Figure 7).

To gain insight into the reactivity of **a-μH-SH**, we have characterized the transition state structure (**TS4**, Figure 6) corresponding to the H_2 evolution path. The free energy barrier for H_2 release from **a-μH-SH** is as large as 17.8 kcal mol^{-1}, indicating that **a-μH-SH** is a long-lived species and therefore corroborates its assignment to the μ-CO species observed experimentally during process I.[12,13] Similar results were obtained when calculations were carried out on di-iron complexes where PDT was substituted with ethane-1,2-dithiolate (EDT, data not shown), in agreement with the experimental observation that a μ-CO species is also formed during the electrochemical reduction of EDT di-iron complexes.[13]

Process II: The Diprotonated Anionic Complex A-H$_2^-$. Process II takes place at more negative potentials compared to those of process I, and it should correspond to the one-electron reduction of **A-H$_2$**.[12] The resulting **A-H$_2^-$** species eliminates dihydrogen, leading to the formation of **A$^-$** (Scheme 2). These observations prompted us to investigate the structural properties of the mononegative species **a-μH-SH$^-$** and **a-H$_2^-$**, which can be obtained by adding one electron to the species **a-μH-SH** and **a-H$_2$**, as well as their reactivity in the context of dihydrogen production.

The structure of **a-μH-SH$^-$** resembles its parent compound **a-μH-SH**, the largest difference being observed for the μ-CO group, which is closer to the iron atom bound by two sulfur ligands in **a-μH-SH$^-$** (Figure 8). In the transition state structure for H_2 evolution from **a-μH-SH$^-$** (**TS5**), the SH group of PDT is no more coordinated to the Fe ions. Most importantly, the reaction free energy barrier for H_2 evolution decreases significantly going from **a-μH-**SH to **a-μH-SH$^-$** (17.8 and 11.9 kcal mol^{-1}, respectively). Moreover, from a thermodynamic perspective, H_2 release from **a-μH-SH$^-$** is extremely favorable ($\Delta G < -25$ kcal mol^{-1}).

The structure of **a-H$_2^-$** (see Figure 8), which is less stable than **a-μH-SH$^-$** by 9.5 kcal mol^{-1}, shows a lengthening of Fe−Fe and H−H distances relative to the neutral species **a-H$_2$**. The free energy barrier for the reaction **a-H$_2^-$** → **a$^-$** + H_2, which goes through the transition state **TS6** (Figure 8), is very small (1.2 kcal mol^{-1}), thus indicating that the

monoelectronic reduction of **a-H$_2$** should be easily followed by dihydrogen evolution, in agreement with the experimental observations indicating that H_2 release is more efficient according to process II than according to process I.[12,13]

Calculation of Redox Potentials. The availability of high quality voltammetry data on the hexacarbonyl di-iron complex allowed us to carry out *in silico* simulations of the electrocatalytic process of proton reduction.[12,13] Results indicated that the redox potential associated with the reduction reaction $\mathbf{A} + e^- \rightarrow \mathbf{A}^-$ should have an intermediate value ($E_{\mathbf{A/A}^-} = -1.2$ V) relative to the potentials of the **A-H**/**A-H**$^-$ and **A-H$_2$**/**A-H$_2$**$^-$ couples ($E_{\mathbf{A-H/A-H}^-} = -1.1$ V; $E_{\mathbf{A-H_2/A-H_2}^-} = -1.45$ V).

In the present work, we have computed the redox potentials for several reduction processes involved in the H_2 evolving cycle (all potentials in this paper are referenced to the SCE to allow the comparison with experimental data, see Methods section); the resulting computed values (E^{calc}) were used to evaluate the tendency of the various di-iron species to undergo a monoelectronic reduction reaction and make a qualitative comparison with the corresponding values obtained from cyclic voltammetry.[12,13]

According to our results, the three key species formed in process I are **a**, **a-μH**, and **a-μH-SH**. The one-electron redox potential for the reduction of **a-μH** to **a-μH**$^-$ was computed[30] to be less negative ($E^{calc}_{\mathbf{a-\mu H/a-\mu H}^-} = -1.16$ V) than the E^{calc} value obtained for **a/a**$^-$ ($E^{calc}_{\mathbf{a/a}^-} = -1.26$ V), in full agreement with experimental observations (Table 2).[12,13]

The accumulation of **a-μH-SH** during cyclic voltammetry experiments requires this species to be stable at the potentials typical of process I ($-1.1/-1.2$ V). Notably, the computed redox potential value for **a-μH-SH** is significantly more negative than the calculated reduction potential for the **a/a**$^-$ couple ($E^{calc}_{\mathbf{a-\mu H-SH/a-\mu H-SH}^-} = -1.50$V), indicating that **a-$\mu$H-SH** should not undergo a reduction reaction at the moderate potentials typical of process I. Analogous conclusions can be drawn when the EDT analogue of **a-μH-SH** is considered ($E^{calc} = -1.42$V).

Conclusions

$Fe_2(S_2C_3H_6)(CO)_6$ is one of the simplest and most studied functional Fe-hydrogenase models. However, several key issues, such as the structure of key intermediate species and the reaction mechanism leading to H_2 production, remained obscure. The DFT dissection of the electrocatalytic H_2 production mediated by $Fe_2(S_2C_3H_6)(CO)_6$ has allowed us to obtain a refined and detailed picture of the chemistry relevant for the H_2 evolving process (Scheme 5): (i) Monoelectron reduction and protonation of the parent species **a** yields a complex characterized by a hydride ligand bridging the metal centers (**a-μH**), which corresponds to the experimental species characterized as **A-H**. Moreover, DFT results allow us to exclude the assignment of the μ-CO species characterized by FT-IR to complex **A-H**. (ii) Further reduction and protonation leads to **a-μH-SH**, which is characterized by both μ-H and μ-CO groups. The IR spectrum of the experimentally characterized μ-CO species is compatible with the diprotonated adduct **a-μH-SH**, which is a relatively long-lived species, in agreement with experimental results.[12,13] (iii) In parallel with the formation of **a-μH-SH**, a less stable isomer characterized by two terminally coordinated H atom is formed (**a-H$_2$**). Release of H_2 from both **a-μH-SH** and **a-H$_2$** is kinetically hindered, in full agreement with experimental data indicating that H_2 evolution from **A-H$_2$** according to process I is a slow process.[12,13] (iv) Monoelectron reduction of **a-μH-SH** and **a-H$_2$** gives place to anionic compounds (**a-μH-SH**$^-$ and **a-H$_2$**$^-$), which are more efficient in H_2 production, in agreement with experimental results.

In light of recent findings indicating that di-iron complexes featuring a terminal hydride ligand which are very reactive toward protons,[31] efforts aiming at the synthesis of adducts with structural and electronic properties similar to those of **a2-H** (as opposed to hydride-bridged isomers such as **a-μH**) could assume great relevance for the development of better electrocatalytic materials, as recently observed also by Rauchfuss, Darensbourg, and Hall.[31,32]

Acknowledgment. We thank Professors C. J. Pickett and S. P. Best for advice and discussions. We gratefully acknowledge CINECA for computing time.

Supporting Information Available: Details related to the validation of the computational approach, linear fitting of calculated and experimental CO frequencies for the **A**$^-$ adduct, optimized structures of **a-SH**, **a1-H**, **a-2H**$^-$, and **a3-H**$^-$, molecular geometry of the transition state structure for H_2 evolution from **a-H$_2$**, as obtained within the broken symmetry formalism, linear fitting between the calculated CO frequencies for **a-η^2-H$_2$** and the corresponding experimental data, optimized structure of **TS3**. This material is available free of charge via the Internet at http://pubs.acs.org.

IC061168+

(30) Calculation of redox potential values for **a/a**$^-$ and **a-μH/a-μH**$^-$ couples led to very similar results (±0.04 V) when geometry optimizations were carried out using a TZVP basis augmented with an additional set of s and p diffuse functions on all heavy atoms (i.e., Fe, C, S, O atoms). This shows that the TZVP basis set is well suited for the description of $Fe_2(S_2C_3H_6)(CO)_6$ monoanionic derivatives.

(31) van der Vlugt, J. I.; Rauchfuss, T. B.; Whaley, C. M.; Wilson, S. R. *J. Am. Chem. Soc.* **2005**, *127*, 16012.
(32) Tye, J. W.; Darensbourg, M. Y.; Hall M. B. *Inorg. Chem.* **2006**, *45*, 1552.